JACS
JOURNAL OF THE AMERICAN CHEMICAL SOCIETY

Article

pubs.acs.org/JACS

New Reactions of Terminal Hydrides on a Diiron Dithiolate

Wenguang Wang, Thomas B. Rauchfuss,* and Lingyang Zhu

School of Chemical Sciences University of Illinois - Urbana, Urbana, Illinois 61801, United States

Giuseppe Zampella*

Department of Biotechnology and Biosciences, University of Milano-Bicocca 20126 Milan, Italy

Supporting Information

ABSTRACT: Mechanisms for biological and bioinspired dihydrogen activation and production often invoke the intermediacy of diiron dithiolato dihydrides. The first example of such a $Fe_2(SR)_2H_2$ species is provided by the complex $[(term\text{-}H)(\mu\text{-}H)Fe_2(pdt)(CO)(dppv)_2]$ ($[H\mathbf{1}H]^0$). Spectroscopic and computational studies indicate that $[H\mathbf{1}H]^0$ contains both a bridging hydride and a terminal hydride, which, notably, occupies a basal site. The synthesis begins with $[(\mu\text{-}H)Fe_2(pdt)(CO)_2(dppv)_2]^+$ ($[H\mathbf{1}(CO)]^+$), which undergoes substitution to afford $[(\mu\text{-}H)Fe_2(pdt)(CO)(NCMe)(dppv)_2]^+$ ($[H\mathbf{1}(NCMe)]^+$). Upon treatment of $[H\mathbf{1}(NCMe)]^+$ with borohydride salts, the MeCN ligand is displaced to afford $[H\mathbf{1}H]^0$. DNMR (EXSY, SST) experiments on this complex show that the terminal and bridging hydride ligands interchange intramolecularly at a rate of 1 s^{-1} at −40 °C. The compound reacts with D_2 to afford $[D\mathbf{1}D]^0$, but not mixed isotopomers such as $[H\mathbf{1}D]^0$. The dihydride undergoes oxidation with Fc^+ under CO to give $[\mathbf{1}(CO)]^+$ and H_2. Protonation in MeCN solution gives $[H\mathbf{1}(NCMe)]^+$ and H_2. Carbonylation converts $[H\mathbf{1}H]^0$ into $[\mathbf{1}(CO)]^0$.

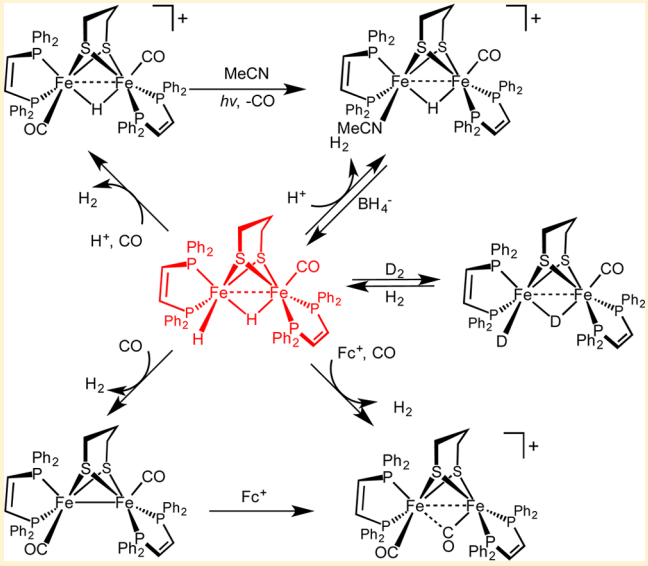

INTRODUCTION

For several years, diiron hydrides have been heavily studied because they are intermediates in the enzymatic production and oxidation of H_2 by enzymes.[1] Since these enzymes are so efficient and so fast, many model complexes have been synthesized to mimic aspects of this catalysis. Focusing on the hydride intermediates, the greatest challenge in the modeling area is the tendency of the terminal hydrides, with the connectivity Fe−Fe−H, to isomerize to bridging hydrides, with the connectivity Fe−H−Fe (Figure 1). Indeed the $Fe_2(\mu\text{-}H)$ entity is predicted to be unusually stable.[2] In the [FeFe]-hydrogenase, it appears that supramolecular interactions prevent this isomerization, but in models, the isomerization can only be slowed (but not stopped) by sterically inhibiting the rotation at the FeH center.[3,4] This paper describes a new approach to the "terminal hydride problem"—incorporate *both* terminal and bridging hydrides into such diiron complexes.

Several diiron di- and polyhydrides have been investigated,[5] and this situation is poised to accelerate in step with the interest in catalysis by first row metals.[6] Examples include diiron(III) di- and polyhydrides, e.g., $Cp^*_2Fe_2(\mu\text{-}H)_4$,[7] and diiron(II) dihydrides,[8] e.g., $H_2Fe_2(NacNac)_2$.[9] Polyiron di- and polyhydrides are implicated in other areas of homogeneous catalysis[5] including nitrogenase.[10] With few exceptions,[11] the hydride ligands bridge the metal centers. Although diiron *dithiolato* dihydrides have not been described,[12] they are implicated in proton reduction catalysis (hydrogen evolution reaction, or HER) by bioinspired catalysts.[13] Di- and even trihydrides of diiron dithiolates are also implicated in the

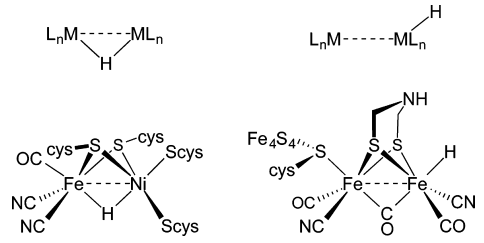

Figure 1. *(Left)* "Bridging hydride structure" proposed for active site of [NiFe]-hydrogenase. *(Right)* "Terminal hydride structure" proposed for active site of [FeFe]-hydrogenase in H_{red} state.

Received: February 8, 2014
Published: March 22, 2014

dx.doi.org/10.1021/ja501366j | J. Am. Chem. Soc. 2014, 136, 5773−5782

Scheme 1. Synthesis and Reactions of $[(t\text{-H})(\mu\text{-H})Fe_2(pdt)(CO)(dppv)_2]$ ($[H1H]^0$)

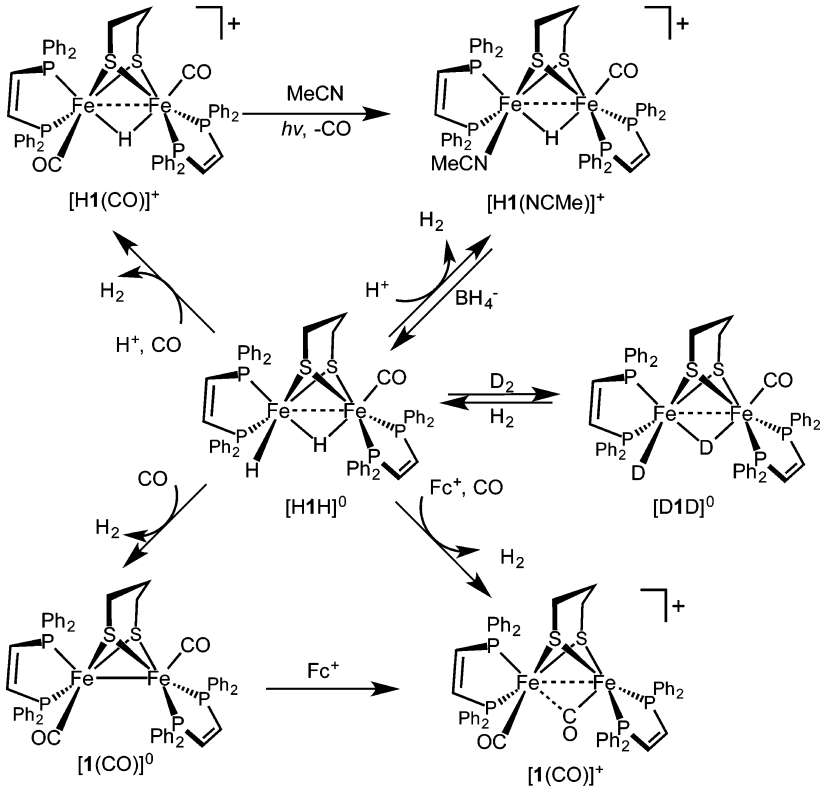

exchange between H_2 and D_2 photocatalyzed by $[HFe_2(pdt)(CO)_4(PMe_3)_2]^+$.[14]

RESULTS AND DISCUSSION

Dihydride $[(t\text{-H})(\mu\text{-H})Fe_2(pdt)(CO)(dppv)_2]$. The synthesis and reactions of the new diiron dihydride, $[(t\text{-H})(\mu\text{-H})Fe_2(pdt)(CO)(dppv)_2]$ ($[H1H]^0$) are outlined in Scheme 1.

The synthetic approach exploits the lability of CO ligands in the cationic diferrous hydride $[(\mu\text{-H})Fe_2(pdt)(CO)_2(dppv)_2]^+$ ($[H1(CO)]^+$). Photolysis of MeCN solutions of this dicarbonyl resulted in clean monosubstitution, affording $[(\mu\text{-H})Fe_2(pdt)(CO)(MeCN)(dppv)_2]^+$ ($[H1(NCMe)]^+$). For this cation ν_{CO} = 1942 cm^{-1}, which can be compared with 1952 (s) and 1972 (sh) cm^{-1} in $[H1(CO)]^+$. As in $[H1(CO)]^+$, the ^{31}P NMR spectrum of $[H1(NCMe)]^+$ indicates two isomers in a 90:10 ratio. In the major isomer, labeled *ab*–*bb*, one dppv occupies apical and basal sites (*ab*) and the other dppv occupies the two basal sites (*bb*) on the other Fe center. The MeCN ligand occupies only one of two nonequivalent sites. In the minor (13%) isomer of $[H1(NCMe)]^+$, both dppv ligands are disposed in the *ab* mode and the MeCN binds to one of two equivalent basal sites in this *ab*–*ab* isomer. This isomer displays four ^{31}P NMR signals.

The structure of a major isomer of $[H1(NCMe)]BF_4$ was confirmed crystallographically (Figure 2). The MeCN ligand occupies a basal position. The bridging hydrido ligand, the location of which was identified in the difference map, refined to a position slightly closer to the Fe(NCMe) center (1.63(2) Å) than to the Fe(CO) site (1.72(2) Å). In contrast, the two Fe–H distances in $[H1(CO)]^+$ are almost identical with values of 1.65 (3) and 1.68 (3) Å.[7]

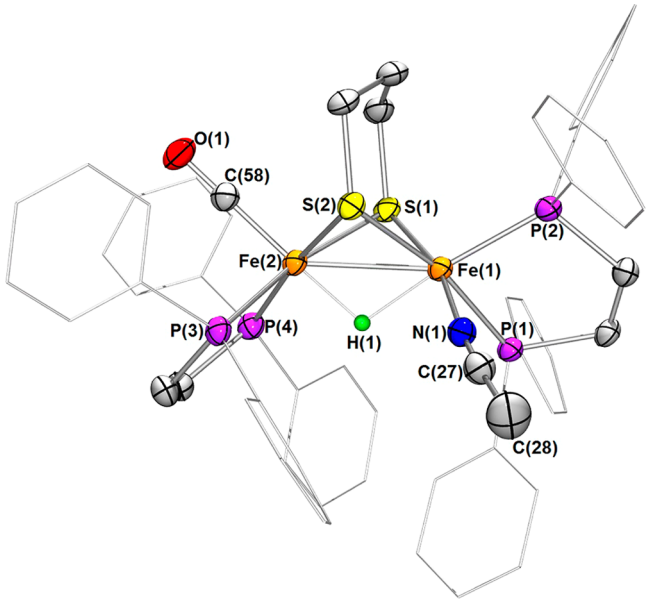

Figure 2. Structure of major *ab*–*bb* isomer of $[H1(NCMe)]^+$. Counterion (BF_4^-) and solvent of crystallization are not shown. Thermal ellipsoids set at the 50% probability level. For clarity, phenyl groups are drawn as lines and hydrogen atoms (except the hydride ligand) are omitted. Selected distances (Å): Fe(1)–Fe(2), 2.6549(4); Fe(1)–H(1), 1.72(2); Fe(2)–H(1), 1.63(2); Fe(1)–S_{avg}, 2.2555(5); Fe(2)–S_{avg}, 2.2674(5); Fe(1)–P(1), 2.2502(5); Fe(1)–P(2), 2.2195(6); Fe(2)–P(3), 2.2093(5); Fe(2)–P(4), 2.2334(5); Fe(1)–N(1), 1.9328(16); N(1)–C(27), 1.134(2). Angles (deg): S(1)–Fe(1)–S(2), 84.013(18); S(1)–Fe(2)–S(2), 83.471(19); Fe(1)–Fe(2)–H(1), 38.9(7); Fe(2)–Fe(1)–H(1), 36.4(7).

dx.doi.org/10.1021/ja501366j | J. Am. Chem. Soc. 2014, 136, 5773–5782

The MeCN ligand in $[H1(NCMe)]^+$ is displaced by a hydride donated by NBu_4BH_4 to afford the targeted complex $[H1H]^0$, isolated as a green toluene-soluble solid. The ν_{CO} band for this complex is found at 1915 cm^{-1} (Figure 3). This complex is stable at room temperature but is susceptible to a variety of thermally and chemically induced reactions as described below.

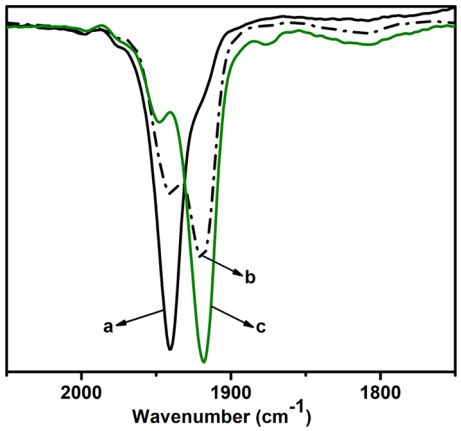

Figure 3. IR spectra in ν_{CO} region for (a) $[H1(NCMe)]BF_4$ in THF solution after treatment with one equiv of solid $[NBu_4]BH_4$ for (b) 1 min, and (c) 10 min.

Attempted preparation of the related dihydride $[H_2Fe_2(pdt)(dppv)(CO)_3]$ failed because the precursor $[(\mu\text{-}H)Fe_2(pdt)(CO)_3(NCMe)(dppv)]^+$ oxidizes borohydride. This result can be rationalized qualitatively on the basis of redox potentials: the (irreversible) oxidation BH_4^- is −1.64 V (−1.24 V vs SHE[15]) and the couple $[(\mu\text{-}H)Fe_2(pdt)(CO)_3(NCMe)(dppv)]^{+/0}$ is the relatively mild −1.38 V vs $Fc^{+/0}$ (Supporting Information [SI]). In contrast, the $[H1(NCMe)]^{+/0}$ is −1.83 V. Indeed, treatment of the tricarbonyl cation with NBu_4BH_4 gave ∼50% the reduced species $Fe_2(pdt)(CO)_4(dppv)$ as well as other unidentified species.

The structure of $[H1H]^0$ was initially assigned on the basis of its NMR properties. The room temperature ^1H NMR spectrum features broad peaks around δ −12 and −19. These signals sharpen at lower temperatures (T < 0 °C). At −40 °C, well-resolved peaks are observed at δ −12.2 and −18.9. The δ −12.2 signal appears as a quartet with $J_{P-H} \approx 24$ Hz. The upper field signal δ −18.90 appears as a triplet, with $J_{P-H} \approx 62$ Hz. Four signals are observed in the $^{31}P\{^1H\}$ NMR spectrum: doublets at δ 108 (d, J_{P-P} = 56.5 Hz) and 105 (d, J_{P-P} = 56.5 Hz) and singlets at δ 80.6 and 77.9. Typically apical−basal dppv ligands exhibit ^{31}P NMR signals above δ 90, whereas dibasal dppv ligands absorb below δ 90.[16] In the two-dimensional (2D) $^{31}P-^{31}P$ TOCSY experiment, cross-peaks are only observed between the apical−basal dppv signals at δ 108 and 105. No $^{31}P-^{31}P$ interaction was observed within the dibasal dppv (SI).

The structure of $[H1H]^0$ was further examined by 2D $^1H-^{31}P$ HMBC (heteronuclear multiple-bond correlation) spectroscopy. In the HMBC spectrum (Figure 4), with the use of the long-range coupling of 60 Hz, three cross-peaks are observed: between the hydride at δ −12.2 and the phosphorus (δ 105, 80.6, and 77.9), and two cross-peaks between the hydride at δ −18.9 and the phosphorus (δ 108 and 105). These results indicate that the ^1H signal at δ −12.2 is coupled to three ^{31}P signals (δ 105, 80.6, and 77.9), and the ^1H signal at δ −18.9

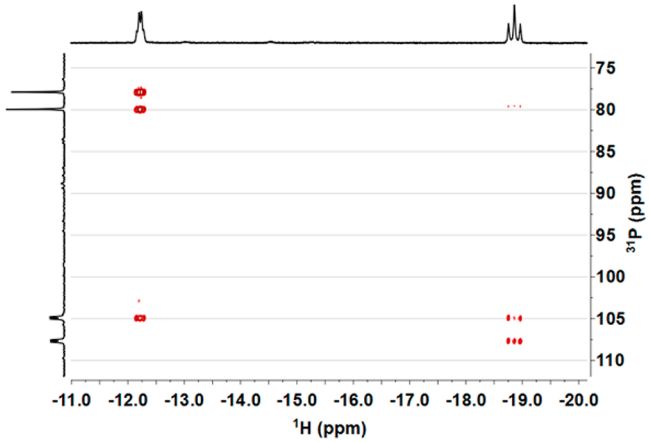

Figure 4. $^1H-^{31}P$ HMBC spectrum of $[H1H]^0$ in THF-d_8 at −40 °C. The multibond J_{H-P} was set to 60 Hz.

is coupled to two ^{31}P NMR signals (δ 108 and 105). These results are consistent with the assignment of the ^1H NMR signal at δ −12.2 to the bridging hydride, and the signal at δ −18.9 to the terminal hydride. The relative chemical shifts of the hydride signals are reversed from the usual pattern of terminal hydrides being lower field than bridging hydrides in diiron dithiolates compounds,[3] but the usual trend may only apply to terminal, *apical* hydrides. In addition, based on the J_{P-H} coupling value of ∼62 Hz obtained in the ^1H NMR spectrum, this terminal hydride is cis to the two phosphorus centers (δ 108 and 105). As repeatedly observed in related complexes[3] and in simpler iron phosphine hydride complexes, two-bond $^1H-^{31}P$ couplings are characteristically large when these nuclei are mutually cis.[17] Overall, the pattern in HMBC spectrum is consistent with a terminal, basal hydride (δ −18.9) and a hydride (δ −12.2) that bridges *a,b-* and *b,b*-Fe(dppv) centers. Coupling between the two hydride centers is not observed. In mononuclear complexes this coupling constant can be small.[18] These assignments lead to the structure shown in Figure 5.

Structure of $[H1H]^0$. Since $[H1H]^0$ did not crystallize suitably, its structure was examined by DFT calculations. As the DFT scheme, we adopted B-P86/TZVP, one of the best performers (even better than the very popular B3LYP) in reproducing the crystallographic parameters as well as IR spectra ($\nu_{CO/CN}$) of active-site mimics of the [FeFe] and

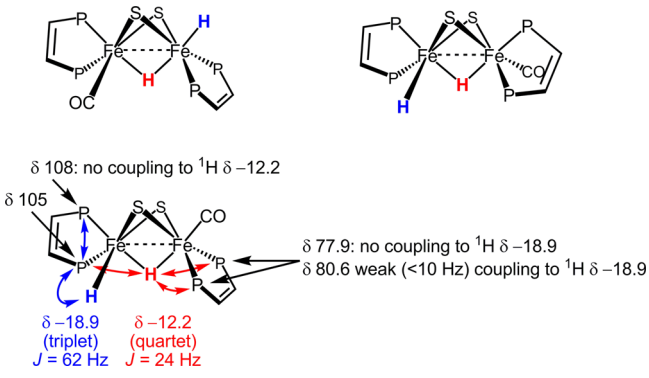

Figure 5. Connectivity for three possible isomers of the $H_2Fe_2S_2(CO)(P_2C_2H_2)_2$ core of $[H1H]^0$ with nonequivalent phosphorus centers. The proposed isomer is shown with NMR assignments.

dx.doi.org/10.1021/ja501366j | J. Am. Chem. Soc. 2014, 136, 5773−5782

[NiFe] hydrogenase,[19,20] even if this success may be partially attributable to the effect of error cancellation.[21] Our calculations indicate that the isomer with a basal terminal hydride is 2 kcal/mol lower in energy than the isomer with the more precedented apical terminal hydride. Despite this small calculated energy difference, no evidence experimentally was observed for a second isomer. Previous DFT calculations had predicted that apical and basal hydrides may be quite close in energy in other diiron dithiolates.[22] Qualitatively, the proposed structure is consistent with the general trend that μ-hydride ligands prefer weak donors or strong acceptors at the two trans (apical) sites. Although the complex's stereochemistry is noteworthy, the calculated bond distances and angles are unremarkable (Figure 6).

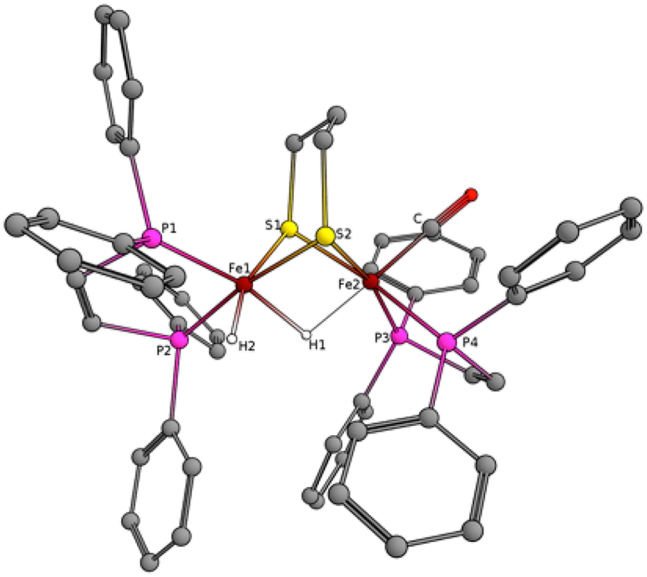

Figure 6. DFT-Calculated structure of $[H1H]^0$. Distances in Å: Fe1–H1, 1.673; Fe1–H2, 1.527; Fe1–P1, 2.175; Fe1–P2, 2.200; Fe1–S1, 2.270; Fe1–S2, 2.255; Fe2–C, 1.748; Fe2–H1, 1.750; Fe2–P3, 2.248; Fe2–P4, 2.251; Fe2–S1, 2.321; Fe2–S2, 2.286.

The isosurface of the HOMO (Figure 7) shows qualitatively that bridging and terminal basal hydrides should feature different chemical properties. This mapping indicates that the basal-H should be more nucleophilic and more basic than the bridging hydride.[23]

DFT was also used to calculate IR and NMR spectra for all structures reported in Figure 5. The DFT-calculated value of ν_{CO} is 1923 cm^{-1}, vs 1915 cm^{-1} observed. The deviation is attributed to the harmonic approximation employed in all quantum chemistry program codes.[24] The DFT-calculated value of ν_{CO} for the apical hydride isomer of $[H1H]^0$ is 1930 cm^{-1}. According to the calculations, ν_{C-O} is weakly coupled with the Fe–H_{ba} and Fe–H–Fe vibrations. Consistent with weak coupling between CO and Fe-H/D modes, for $[D1D]^0$, ν_{CO} = 1919 cm^{-1}, 4 cm^{-1} shift. Calculations predict a 1 cm^{-1} shift. Moreover, in the DFT-calculated IR spectrum of $[D1D]^0$, the vibronic coupling, observed in $[H1H]^0$ for ν_{C-O} and Fe–H modes, disappears.

For the DFT-calculated NMR data, the model was simplified by replacing Ph with methyl groups. The calculations reproduce the chemical shifts for the hydride ligands, predicting δ −19.5 and −12.9 for the terminal and bridging hydrides, respectively. The agreement between the chemical shifts calculated for the

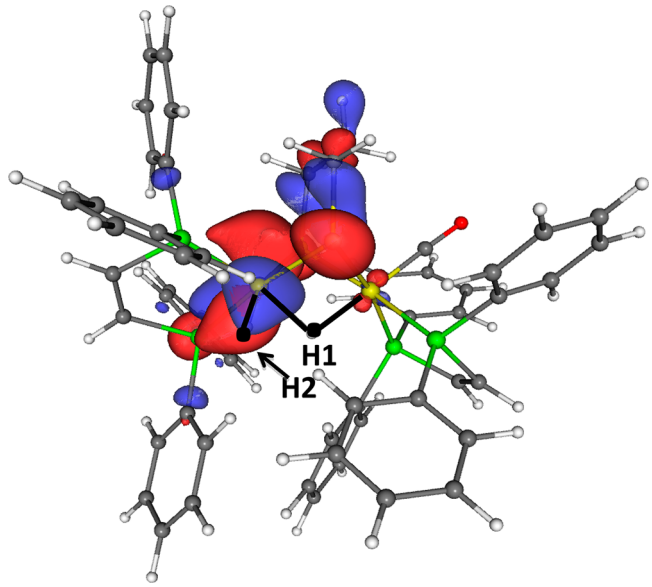

Figure 7. DFT-calculated HOMO for $[H1H]^0$ with isosurface value of 0.02 showing that the basal hydride ligand is embedded in this orbital. The NBO partial charge calculations indicate $q_{bridging\text{-}H}$ = −0.14 and $q_{basal\text{-}H}$ = −0.16.

terminal basal hydride is noteworthy because previous examples of terminal (apical) hydrides absorb near δ −4.[3] For the isomeric structure (Figure 5) with the terminal hydride, the hydrides absorb at δ −12.3 and −12.4. The ^{31}P NMR spectra observed for $[H1H]^0$ and calculated for the analogous $(Me_2PCH{=}CHPMe_2)_2$ complex do not agree, but such shifts are known to be very sensitive to alkyl vs aryl substituents on P. Nonetheless, calculated ^{31}P chemical shifts are qualitatively more consistent on the basal hydride assignment (SI).

Hydride Interchange in $[H1H]^0$. Insight into the exchange between the hydride sites was obtained by a combination of ^1H–^1H 2D EXSY and 1D ^1H spin saturation transfer (SST) experiments. At −40 °C, the 2D EXSY spectrum (mixing time of 300 ms, see SI) shows an intense cross-peak linking the signals at δ −12.2 and −18.9. This cross-peak has the same sign as the diagonal peaks, indicating it arises from chemical exchange of the two hydrides (cross-peaks from nuclear Overhauser enhancement (NOE) take the opposite sign of the diagonal peaks). In spin saturation transfer experiments, presaturation (continuous low-power irradiation) of the hydride resonance at δ −18.9 leads to selective loss of intensity of the signal at δ −12.2 and vice versa. Other peaks were unaffected. As shown in Figure 8, the rate of exchange between the hydride sites is indicated by the time dependence of the intensity of the bridging hydride resonance (at δ −12.2) as a function of the duration (τ) of presaturation at δ −18.9. The rate constant for H/H exchange, $k = 1/\tau$, was calculated to be 1.14 s^{-1} by fitting these data. This reverse rate constant (saturated at δ −18.9, observed δ −12.2) was fit to be 0.91 s^{-1}, which is close to 1.14 s^{-1} for the forward rate.

The rate of H–H exchange was found to be independent of concentration of the diiron complex. For the sample concentration from 24 to 8 mM, the rate constants for hydride exchange were almost the same (0.91 and 0.88 s^{-1}) by presaturation of resonances at δ −18.9 and −12.2, respectively. These rate constants are within 20% of the values found for the

dx.doi.org/10.1021/ja501366j | J. Am. Chem. Soc. 2014, 136, 5773–5782

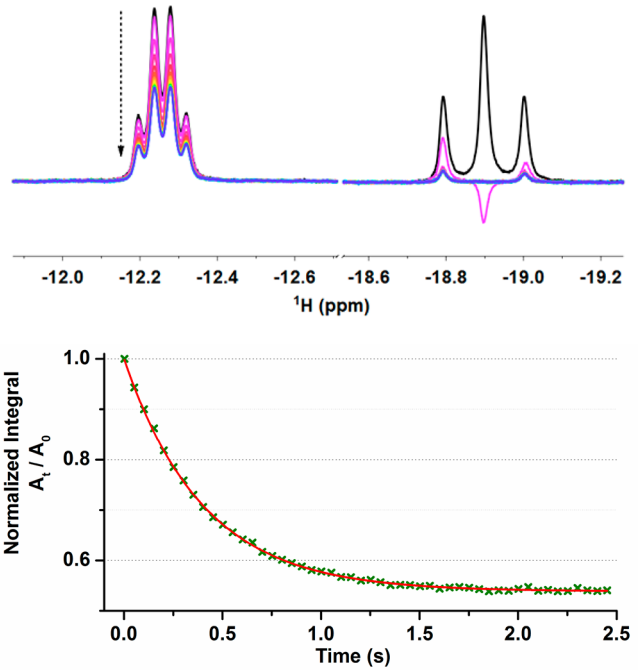

Figure 8. Spin saturation transfer spectra of $[H1H]^0$ at −40 °C in THF-d_8 (sample concentration: 24 mM), showing the decay of the hydride signal at δ −12.2 upon irradiating the hydride resonance at δ −18.9 (top), and the plot of decay vs presaturation time at δ −12.2 (bottom). The presaturation time was increased by 0.05 s for each successive measurement. Fitting results: $A_t/A_0 = 1/(1 + \tau/0.748) \times \exp[-t \times (1/0.748 + 1/\tau)] + 1/(1 + 0.748/\tau)$, τ = 0.874 s, where τ is lifetime $(1/k)$ for the exchanging H at δ −12.2.

more concentrated solution, indicative of an intramolecular mechanism for exchange.

The spin saturation transfer measurements at various temperatures between −60 to 0 °C were acquired (Figure 9).

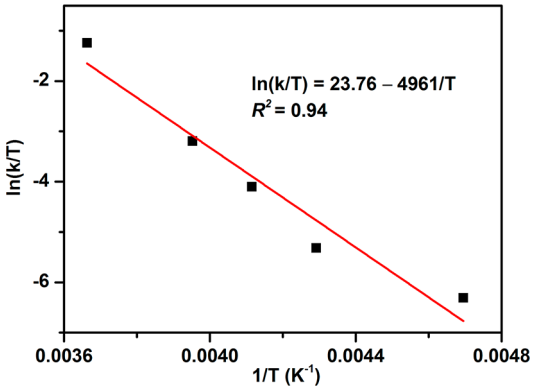

Figure 9. Eyring plot of H/H exchange for $[H1H]^0$ taken from SST data. *Results*: $\Delta H^{\ddagger}$ = +41.2 (±0.8) kJ/mol, $\Delta S^{\ddagger}$ = −60 (±3.4) J/K·mol.

The rate constant k increases from 0.387 s^{-1} (−60 °C) to 79.0 s^{-1} at 0 °C. The activation energy for the exchange process was determined to be 43.2 kJ/mol, and the temperature dependence of k gives $\Delta H^{\ddagger}$ = +41.2 (±0.8) kJ/mol, $\Delta S^{\ddagger}$ = −60 (±3.4) J/K·mol (Figure 9).

The ^{31}P−^{31}P 2D EXSY spectrum recorded at various mixing times in the range of 50−500 ms showed no cross-peaks, indicating the slowness of site exchange at −40 °C. Together with the ^{1}H DNMR data that indicate that interchange of the hydrides occurs at ∼1 s^{-1} (−40 °C), the ^{31}P−^{31}P 2D EXSY result suggests that H−H exchange occurs without symmetrizing the complex. A pathway consistent with this finding is shown in eq 1.

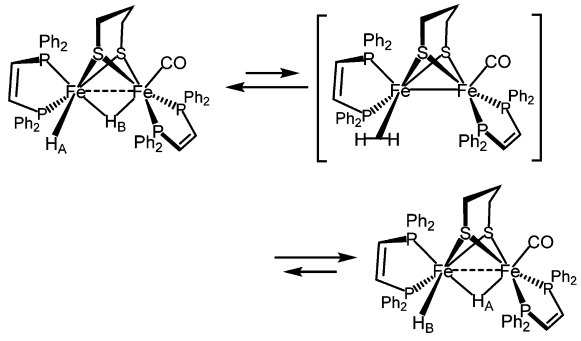

(1)

The D/D exchange rate was evaluated for $[D1D]^0$, which was prepared by the reaction of D_2 with $[H1H]^0$ (see below). Although the ^{31}P NMR chemical shifts are almost identical for $[H1H]^0$ and $[D1D]^0$, the coupling patterns are fairly distinctive. Four signals were observed: broad doublet−multiplets (dm, 44.9 Hz) at δ 80.0 and at 77.9 as well as broad singlets at δ 108 and 105. The D/D exchange rate at −40 °C was determined to be 7.89 s^{-1} vs 1.14 s^{-1} for H/H exchange in $[H1H]^0$ (^{2}H-SST was used to determine the exchange rate since the signals are weak in the EXSY experiment). As examined by DFT methods, the low-energy pathway for H−H exchange is proposed to proceed via a transition state with an H−H-bonding interaction (r_{H-H} = 0.996 A, eq 1). The barrier is 10.3 kcal/mol, which nicely reproduces the experimental value. Aside from the Fe−H and H−H distances, no other bonds change by >0.02 Å relative to the ground-state geometry.

Attempts were made to obtain the monodeuteride $[(t\text{-}H)(\mu\text{-}D)Fe_2(pdt)(CO)(dppv)_2]$ by treatment of $[D1(NCMe)]^+$ with BH_4^-. The product proved to be a mixture of not only $[D1H]^0$/$[H1D]^0$ but also $[H1H]^0$ (and we assume $[D1D]^0$), as indicated by 2-D EXSY measurements that showed cross peaks for exchange between the ^{1}H sites.

The interchange of terminal and bridging hydrides has been demonstrated in the case of $Cp^*_2Fe_2(term\text{-}H)(\mu\text{-}H)(PPh_2)_2$ and $(term\text{-}H)(\mu\text{-}H)Os_3(CO)_{11}$.[7,25] In the latter case, exchange is proposed to occur via an intermediate where both hydrides are terminal.[25] This mechanism does not appear to apply to $[H1H]^0$, as explained above.

Reductive Elimination of H_2. The reductive elimination from dihydrido complexes is an established route to unsaturated complexes.[26] The reductive elimination of H_2 from $[H1H]^0$ in principle should afford "$Fe_2(pdt)(CO)(dppv)_2$", a 32e$^-$ diiron(I) dithiolate. Such a highly unsaturated species is expected to be reactive. Upon heating in THF, $[H1H]^0$ yields H_2 and a complex mixture of organometallic products, as indicated by ^{31}P NMR analysis. Alternatively, when $[H1H]^0$ was allowed to decompose in the presence of ∼0.5 atm CO, the organometallic product is the well-known species $[1CO]^0$,[3] as indicated by NMR and IR analyses (SI).

Solutions of $[H1H]^0$ also react with D_2 and produce $[D1D]^0$. When the reaction was monitored in a sealed NMR tube, H_2 was observed (δ 4.56, s) together with only ∼10% HD (see SI). The ^{2}H NMR spectrum shows signals at δ −12.2 and −18.9 in THF at −40 °C (Figure 10). The ν_{CO} band slightly shifts from 1915 to 1919 cm^{-1} upon conversion of $[H1H]^0$ to $[D1D]^0$.

dx.doi.org/10.1021/ja501366j | J. Am. Chem. Soc. 2014, 136, 5773−5782

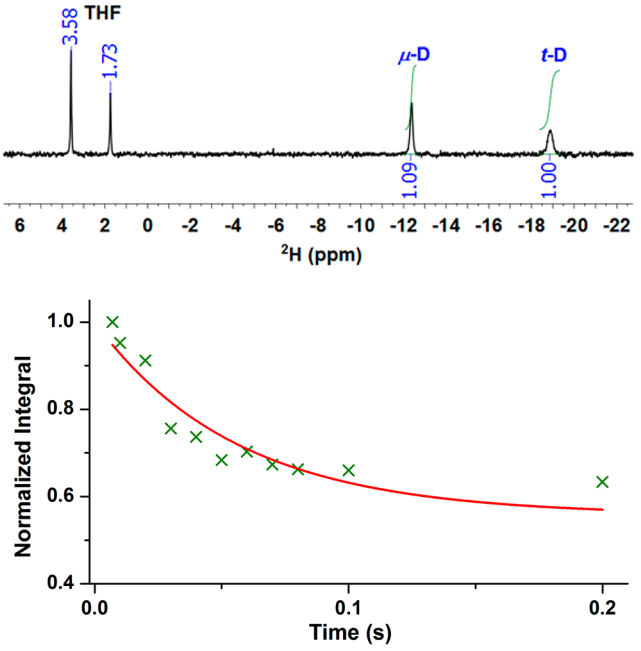

Figure 10. (Top) ^{2}H NMR spectrum of $[\mathbf{1}D\mathbf{1}D]^0$ generated from the reaction of $[\mathbf{1}H\mathbf{1}H]^0$ and D_2 in THF at −40 °C. (Bottom) Plot of decay vs time at δ −12.24 from SST experiments. Fitting results: $A_t/A_0 = 1/(1 + \tau/0.1005) \times \exp[-t \times (1/0.1005 + 1/\tau)] + 1/(1 + 0.1005/\tau)$, τ = 0.1267s.

Protonolysis. In contrast to known hydrides (terminal and bridging) of other diiron dithiolates, $[\mathbf{1}H\mathbf{1}H]^0$ reacts readily with acids with evolution of H_2. With addition of one equivalent of $H(OEt_2)_2BArF_4$, the color of a THF solution of $[\mathbf{1}H\mathbf{1}H]^0$ immediately changed from dark green to brown. Yields of H_2, quantified by GC analysis, approached 95.7% (four experiments, standard deviation of 9.2%). Weak acids such as $PhCO_2H$ (pK_a^{MeCN} = 21.51[27]) also induce hydrogen evolution, although these reactions require a few minutes at room temperature.

The protonolysis of $[\mathbf{1}H\mathbf{1}H]^0$ by $H(OEt_2)_2BArF_4$ was explored under a variety of conditions. When conducted under an atmosphere of CO, $[\mathbf{1}H(CO)]^+$ was regenerated in 87% yield as confirmed by IR as well as ^{1}H and ^{31}P{^{1}H} NMR analyses (eq 2 and Figure 11). Protonation under a ^{13}CO

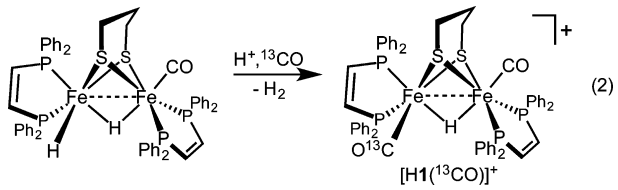

(2)

atmosphere afforded $[\mathbf{1}H(^{13}CO)]^+$ wherein one of the two CO ligands is labeled. For the singly labeled species, the ν_{CO} band at 1953 is unaffected, but the second band shifts from 1971 to 1925 cm^{-1}. The ^{13}C NMR spectrum displays a triplet at δ 218 with J_{P-C} = 15 Hz and a small singlet at δ 212.6 for two CO groups. The ^{31}P NMR spectrum exhibits doublets (J_{C-P} = 18 Hz) at δ 87.4 and 83.8 as well as singlets at δ 82.2 and 76.2. The results show that ^{13}CO ligand is coupled to the *ab* dppv. Overall, it is clear that CO is installed stereoselectively (eq 2). The ESI-MS spectrum of $[\mathbf{1}H^{13}CO]^+$ also confirmed the single label. Protonolysis of $[\mathbf{1}H\mathbf{1}H]^0$ in the presence of MeCN gave $[\mathbf{1}H(NCMe)]^+$. Protonolysis of $[\mathbf{1}D\mathbf{1}D]^0$ under CO in a sealed

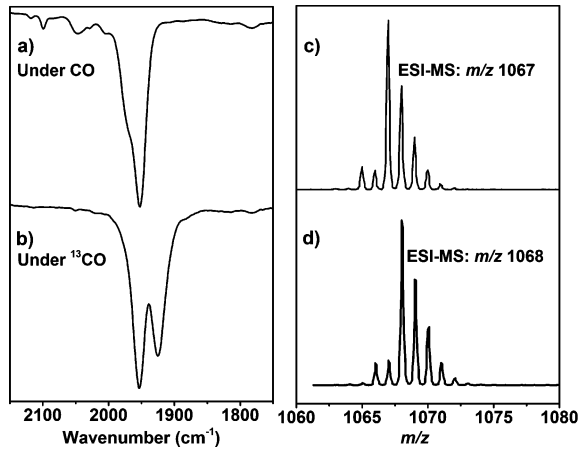

Figure 11. FT-IR spectra in the ν_{CO} region and ESI-MS spectra (([M-$BArF_4$]$^+$) for $[\mathbf{1}H\mathbf{1}H]^0$ in THF solution after treatment with 1 equiv of $H(OEt_2)_2BArF_4$ under CO (a and c), and ^{13}CO (b and d) atmosphere.

NMR tube, a difficult experiment, afforded HD and H_2 in a 2:1 molar ratio and almost exclusively $[\mathbf{1}D\mathbf{1}CO]^+$. Protonolysis of $[\mathbf{1}H\mathbf{1}H]^0$ with $H(OEt_2)_2BArF_4$ under an N_2 atmosphere gave only a complex mixture of products, suggesting that $[\mathbf{1}H(N_2)]^+$, if it forms at all, is unstable.

Oxidation of $[\mathbf{1}H\mathbf{1}H]^0$. According to its cyclic voltammogram (CV), a THF solution of $[\mathbf{1}H\mathbf{1}H]^0$ undergoes a quasi-reversible oxidation at −78 mV (i_{pc}/i_{pa} = 0.52) vs $Fc^{+/0}$ at the scan rate of 100 mV/s. For comparison, the couple $[Fe_2(pdt)(CO)_2(dppv)_2]^{0/+}$ occurs at −360 mV vs Ag/AgCl (−850 mV vs $Fc^{+/0}$ in CH_2Cl_2).[28] The CV of $[\mathbf{1}H\mathbf{1}H]^0$ shows no reductive events out to −2.00 V (vs $Fc^{+/0}$).

The oxidation of $[\mathbf{1}H\mathbf{1}H]^0$ could also be effected by treatment with ferrocinium salts. Addition of one equivalent of $FcBAr^F{}_4$ to $[\mathbf{1}H\mathbf{1}H]^0$ resulted in nearly quantitative release of H_2 (97.6%, four experiments, standard deviation of 1.3%).

Judging from the FT-IR and ESI-MS spectrum analysis, oxidation in the presence of CO afforded $[Fe_2(pdt)(CO)_2(dppv)_2]^+$, $[\mathbf{1}CO]^+$. The Fc^+-induced reaction of $[\mathbf{1}H\mathbf{1}H]^0$ with CO is noticeably faster than the direct carbonylation (see above). In the absence of CO, oxidation produces a complex mixture of organometallic products. The FT-IR spectrum of $[\mathbf{1}CO]^+$ exhibits strong bands at 1885 and 1955 cm^{-1}, assigned to $\nu_{\mu\text{-}CO}$ and $\nu_{t\text{-}CO}$, respectively (Figure 12). The product, $[\mathbf{1}CO]BF_4$, was characterized crystallographically (Figure 13). The cation adopts a highly unsymmetrical, "rotated" structure reminiscent of the H_{ox} state of the [FeFe]-hydrogenase.[28,29] The terminal CO is coordinated to the Fe center with an apical−basal dppv, and the semibridging CO is more strongly bonded to the rotated Fe site. The two Fe-μ-CO distances are very different, being 2.618 ('proximal' Fe1) and 1.786 Å ('distal', rotated Fe1). The bridging CO group is bent with <Fe(2)−C(57)−O(2) = 169.9°.

Oxidation of $[\mathbf{1}H\mathbf{1}H]^0$ under an atmosphere of ^{13}CO afforded $[Fe_2(pdt)(^{13}CO)_2(dppv)_2]^+$ as indicated by ESI-MS. Relative to the spectrum for $[\mathbf{1}CO]^+$ both $\nu_{\mu\text{-}CO}$ and $\nu_{t\text{-}CO}$ are shifted by about 40 cm^{-1} to lower energy. The double labeling arises because such 33e dimers are known to exchange with exogenous CO.[30] For example, a solution of $[\mathbf{1}CO]^+$ under an atmosphere of ^{13}CO atmosphere converts to the doubly labeled derivative in ~30 min. (SI).

Hydride and Hydrogen Transfer from $[\mathbf{1}H\mathbf{1}H]^0$. The hydridic character of $[\mathbf{1}H\mathbf{1}H]^0$ was also demonstrated by its

dx.doi.org/10.1021/ja501366j | J. Am. Chem. Soc. 2014, 136, 5773−5782

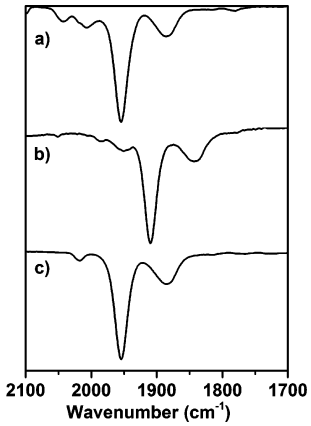

Figure 12. IR spectra of THF solutions of $[H1H]^0$ after addition of $FcBAr^F_4$ under (a) ~0.5 atm CO and (b) ~0.5 atm ^{13}CO. Spectrum (c) is for $[Fe_2(pdt)(CO)_2(dppv)_2]^+$ obtained from treating $Fe_2(pdt)(CO)_2(dppv)_2$ with $FcBAr^F_4$ in THF.

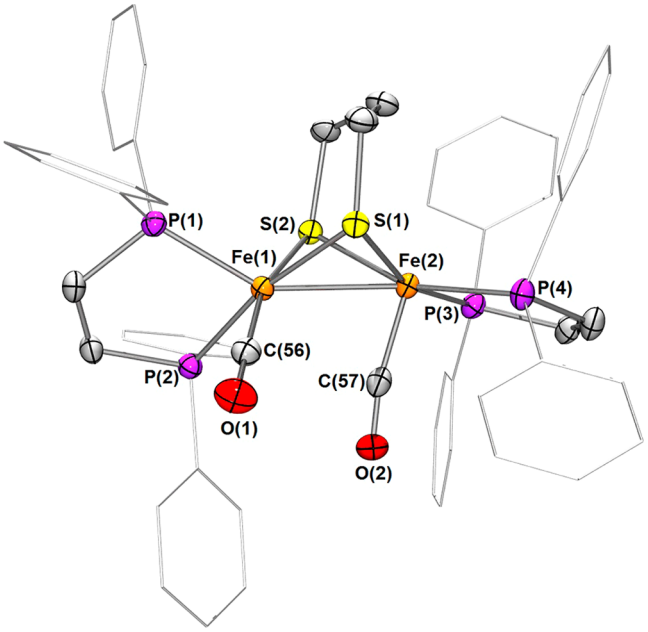

Figure 13. Structure of the cation $[Fe_2(pdt)(CO)_2(dppv)_2]^+$ ($[\mathbf{1}(CO)]^+$). Counterion (BF_4^-) and solvent of crystallization are not shown. Thermal ellipsoids are set at the 50% probability level. For clarity, phenyl groups are drawn as lines and hydrogen atoms are omitted. Selected distances Å: Fe(1)–Fe(2), 2.5942(5); Fe(1)–C(56), 1.750(3); Fe(2)–C(57), 1.786(3). Selected angles (deg): Fe(1)–Fe(2)–C(57), 70.67(8); Fe(2)–Fe(1)–C(56), 109.66(9); Fe(2)–C(57)–O(2), 169.9(2); Fe(1)–C(56)–O(1), 179.2(3).

reactivity toward 1,3-dimethylbenzimidazolium salts. Treatment of this weak hydride acceptor[31] with $[H1H]^0$ produced 1,3-dimethylbenzimidazoline. When the reaction was conducted in the presence of MeCN, $[H1H]^0$ converted to $[H1(NCMe)]^+$. $[H1H]^0$ was, however, found to be unreactive toward PhCHO and CO_2.

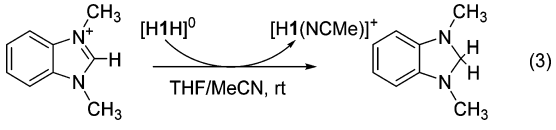

(3)

Solutions of $[H1H]^0$ were also found to react with dimethylacetylenedicarboxylate (DMAD) to give dimethyl maleate (eq 4). The cis stereochemistry of the product is

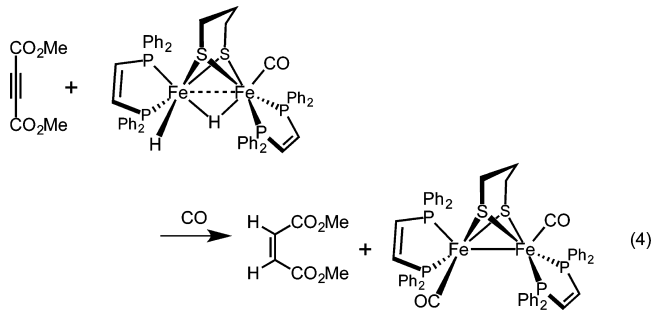

(4)

consistent with a hydrogenation reaction. When this process is conducted under an atmosphere of CO, $[\mathbf{1}CO]^0$ was produced. The DMAD-induced reaction proceeds in minutes at room temperature, whereas the reaction of CO + $[H1H]^0$ to give $[\mathbf{1}CO]^0$ requires hours. Treatment of $[H1H]^0$ with DMAD under an atmosphere of D_2 gave 2,3-dideutero-dimethyl maleate, which implies that this reaction is catalytic.

CONCLUSIONS

The complex $[H1H]^0$ is a unique example of an isolable dihydride derivative of the [FeFe]-hydrogenase mimics. Several mechanistic studies invoke di- or even trihydride intermediates,[1,32] but such species have been unavailable to directly probe their reactivity. Once the targeted dihydride $[H1H]^0$ had been generated, the first question addressed, both computationally and spectroscopically, was its structure. The occurrence of a basal terminal hydride is unprecedented in the chemistry of diiron dithiolates, although basal hydride intermediates are implicated in the conversion of terminal, apical hydrides to μ-hydrides (Scheme 2).[22]

Scheme 2

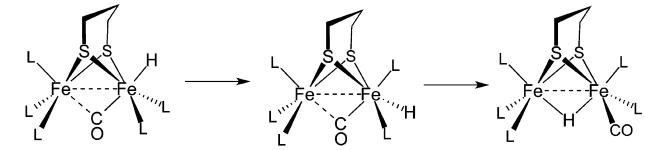

In addition to the calculations and 2D NMR analyses, the basal stereochemistry of the terminal hydride is consistent with the fast intramolecular H/H exchange, a process subject to a substantial inverse isotope effect ($k_H/k_D \approx 0.14$ at −40 °C). This result is consistent with calculations showing the H–H (D–D) bond forms at the transition state for exchange of the hydride sites.[33] Typically, normal kinetic isotope effects ($k_H/k_D > 1$) are observed for the reductive elimination of dihydrides.[33]

The hydridic character of $[H1H]^0$ contrasts starkly with previous examples of diiron hydrides, which are unaffected by mild oxidants and strong acids. For example, $[term\text{-}HFe_2(pdt)(CO)_2(dppv)_2]^+$ requires reduction to undergo protonolysis.[3] In contrast, even weak acids induce H_2 evolution from $[H1H]^0$. The enhanced reactivity of $[H1H]^0$ is attributable to its neutral charge and by the donor strength of the μ-hydride. The complex $[H1H]^0$ is sufficiently hydridic to behave like the "third hydrogenase" (Hmd). In Hmd, a single Fe center

dx.doi.org/10.1021/ja501366j | J. Am. Chem. Soc. 2014, 136, 5773–5782

catalyzes the transfers of hydride to a dihydroimidazolium substrate, one step in the methanogenesis cycle.[34] The emergence of hydride transfer reactivity is manifested also in the hydrogenation of an electrophilic alkyne by $[H\mathbf{1}H]^0$. These reactions may foreshadow the development of bioinspired catalysts for reactions other than H_2/H^+ redox.

Oxidants induce reductive elimination of H_2 from $[H\mathbf{1}H]^0$, resulting in net reduction. With the HOMO strongly localized on the terminal hydride, the oxidatively induced reductive elimination can be envisioned as follows (eqs 5 and 6):

$$H{-}Fe^{II}{-}H{-}Fe^{II} \rightarrow H{-}Fe^{III}{-}H{-}Fe^{II} + e^- \quad (5)$$

$$H{-}Fe^{III}{-}H{-}Fe^{II} + CO \rightarrow Fe^{I}{-}CO{-}Fe^{II} + H_2 \quad (6)$$

The finding that the $Fe^I{-}CO{-}Fe^{II}$ species does not bind H_2 is consistent with our proposal that H_2 activation requires an auxiliary oxidant.[35]

The new compound $[H\mathbf{1}H]^0$ is a precursor to the following highly unsaturated species: the 31e- and 32e-cations $[Fe_2(pdt)(CO)(dppv)_2]^+$ and $[HFe_2(pdt)(CO)(dppv)_2]^+$ and the 32e-neutral species $[Fe_2(pdt)(CO)(dppv)_2]^0$. Oxidation is known to greatly enhance the acidity of hydrides and induce reductive elimination of H_2.[36] Proposed intermediates are trapped as their CO derivatives. It is interesting that these hydrogenase mimics, like the hydrogenases, show no affinity for N_2 despite their high sensitivity toward CO.[37]

EXPERIMENTAL SECTION

Material and Methods. Experimental methods have been recently described.[13] NBu_4BH_4, ^{13}CO and D_2 were purchased from Sigma-Aldrich and used as received. FT-IR measurements (in cm^{-1}) are reported for the ν_{CO} region only.

$[HFe_2(pdt)(CO)(NCMe)(dppv)_2]BF_4$ ($[H\mathbf{1}(NCMe)]BF_4$). A solution of $[H\mathbf{1}]BF_4$ (345 mg, 0.3 mmol)[13] in 100 mL of CH_2Cl_2/MeCN (v/v = 90/10) in a Pyrex Schlenk tube was photolyzed (>400 nm cutoff filter) with a 200 W medium-pressure mercury lamp under argon flow. The reaction was monitored by FT-IR spectroscopy. The color of the reaction mixture changed from brown to black gradually over the course of the reaction. After ~6 h, the solvent was removed under vacuum. The residue was extracted into 10 mL of CH_2Cl_2. The solution was filtered through a plug of Celite, and the filtrate was diluted by 30 mL of diethyl ether, resulting in precipitation of black solid. Yield: 310 mg (88%). ^1H NMR (500 MHz, CD_2Cl_2, 20 °C): δ 8.02−6.05 (m, 44H, 40 × Ar*H*, 2 × $Ph_2PCH{=}CHPPh_2$), 2.55−1.15 (m, 6H, $SCH_2CH_2SCH_2$), 0.93 (s, 3H, CH_3CN), −12.68 (m, 1H, μ-H). $^{31}P\{^1H\}$ NMR (202 MHz, CD_2Cl_2, 20 °C): *ab*−*bb* isomer, δ 96.6 (s), 85 (s), 84.9 (s) and 78 (s); *ab*−*ab* isomer, δ 87.3 (s), 85.4 (s), 84.8 (s) and 82.6 (s). The *ab*−*bb*/*ab*−*ab* ratio is 87:13. FT-IR (THF): 1942. ESI-MS, m/z: 1080.5 ($[M\text{-}BF_4]^+$). Anal. Calcd (found) for $C_{58}H_{54}NBF_4Fe_2OP_4S_2{\cdot}CH_2Cl_2$: C, 56.58 (56.72); H, 4.51 (4.58); N, 1.12 (1.33). Single crystals were obtained by allowing a hexane layer to diffuse into a CH_2Cl_2 solution of $[H\mathbf{1}(NCMe)]BF_4$ at −20 °C.

The compound $[D\mathbf{1}(NCMe)]BF_4$ was prepared analogously from $[D\mathbf{1}(CO)]BF_4$, according to the same procedure of preparing $[H\mathbf{1}(NCMe)]BF_4$. $^{31}P\{^1H\}$ NMR (202 MHz, CD_2Cl_2, 20 °C): ab−ab isomer, δ 94.5 (s), 83 (s) and 76 (s), and with the ratio of 1:2:1; *ab*−*ab* isomer, δ 85.4 (s), 83.4 (s), 82.7 (s) and 80.6 (s). The *ab*−*bb*/*ab*−*ab* ratio is 85:15. FT-IR (THF): 1942.

$[H_2Fe_2(pdt)(CO)(dppv)_2]$ ($[H\mathbf{1}H]^0$). To a solution of $[H\mathbf{1}(NCMe)]BF_4$ (233 mg, 0.2 mmol) in 10 mL of THF was added solution of NBu_4BH_4 (52 mg, 0.2 mmol) in 5 mL of THF over the course of 5 min. The reaction mixture was then stirred at room temperature for 30 min, during which time the solution color changed from virtually black to green. The solvent was removed under vacuum. The residue was extracted into toluene (5 mL × 3). The extracts was filtered through Celite, concentrated, and diluted with 30 mL of pentane, resulting in precipitation of a deep-green solid. Yield: 173 mg (83%). ^1H NMR (500 MHz, THF-d_8, −40 °C): δ 8.04−6.75 (m, 42H, 40 × Ar*H*, $Ph_2PCH{=}CHPPh_2$), 6.30 (m, 1H, $Ph_2PCH{=}CHPPh_2$), 5.76 (m, 1H, $Ph_2PCH{=}CHPPh_2$), 2.13−1.25 (m, 6H, $SCH_2CH_2SCH_2$), −12.2 (q, 1H, J_{P-H} = 24 Hz, μ-H) and −18.9 (t, 1H, J_{P-H} = 62 Hz, *t*-H). $^{31}P\{^1H\}$ NMR (202 MHz, CD_2Cl_2, −40 °C): δ108, 105, 80.6, and 77.9. FT-IR (THF): 1915. Anal. Calcd (found) for $C_{56}H_{52}Fe_2OP_4S_2$: C, 64.63 (64.42); H, 5.04 (5.49).

Reaction of $[H\mathbf{1}H]^0$ with D_2. A THF-d_8 solution of $[H\mathbf{1}H]^0$ was sealed in a J-young tube under 6 psi of D_2. ^1H NMR spectra were recorded at 2 h intervals for several hours. The H_2 produced by the reaction was observed at δ 4.57 (s) together with small amount of HD (~10%). In the ^2H NMR spectrum of the product, signals were found at δ −12.2 and −18.9 in ratio of 1:1. No hydrides signals were observed in the high field range of the ^1H NMR spectrum. Although the ^{31}P NMR chemical shifts are almost identical to those for $[H\mathbf{1}H]^0$, the coupling patterns of the signals differ from those of $[H\mathbf{1}H]^0$. Broad double multiplets (dm, 44.9 Hz) at δ 80.0 and 77.9, as well as broad signals at δ 108 and 105. FT-IR (THF): 1919.

Protonolysis of $[H\mathbf{1}H]^0$ in the presence of CO. A J. Young NMR tube containing $[H\mathbf{1}H]^0$ (15 mg, 0.0144 mmol) and $H(OEt_2)_2BArF_4$ (15 mg, 0.0148 mmol) was cooled in liquid nitrogen and evacuated. About 0.5 mL of THF was transferred on the top of the solids, and the frozen sample was purged with CO (6 psi) or ^{13}CO (~6 psi). Then, the NMR tube was vigorously shaken, and the sample was warmed up to room temperature. During this period, the color of the solution changed from dark green to brown. After reaction, the solvent was removed under vacuum. The residue was redissolved in CD_2Cl_2, and the yields of $[H\mathbf{1}(CO)]^+$ were quantified using $[HFe_2(edt)(CO)_4(PMe_3)_2]BAr^F{}_4$ as an internal integration standard (SI). NMR, ESI-MS, and IR analyses indicated the formation of $[H\mathbf{1}(CO)]^+$ when the protonolysis was conducted under CO, and production of $[H\mathbf{1}(CNMe)]^+$ in the presence of MeCN.

Oxidation of $[H\mathbf{1}H]^0$ in the Presence of CO. The oxidation experiment was conducted similarly to the protonolysis, using $FcBAr^F{}_4$ or $FcBF_4$. After reaction, solvent was removed under vacuum. The residue was washed with hexane (5 mL × 3) and redissolved in CH_2Cl_2. Crystals of $[\mathbf{1}(CO)]BF_4$ were grown by allowing a hexane layer to diffuse into a CH_2Cl_2 solution at −20 °C. The compound was isolated in an estimated yield of 80%. The product was identified as $[\mathbf{1}(CO)]BF_4$ by IR, ESI-MS, and X-ray crystallography.

H_2 Elimination from $[H\mathbf{1}H]^0$ in the Presence of CO. A THF solution of $[H\mathbf{1}H]^0$ in a J. Young NMR tube was frozen, and the tube was evacuated. The frozen sample was purged with CO (6 psi) or ^{13}CO. The sample was warmed to room temperature, the sample was shaken, and the $^{13}P\{^1H\}$ NMR spectra were recorded at 2 h intervals. A new signal appeared at δ 90.7 concomitant with the disappearance of signals at δ 108, 105, 80.6, and 79.7 for $[H\mathbf{1}H]^0$. This new species generated features of ν_{CO} bands at 1896(sh), 1884(s), 1849(sh), and 1838(s) cm^{-1}. According to mass spectrum data (ESI-MS: m/z 1067.4), $[Fe_2(pdt)(CO)(^{13}CO)(dppv)_2]$ was generated.

Hydride Transfer to *N,N*-Dimethylbenzimidazolium from $[H\mathbf{1}H]^0$. A solution of 15 mg (0.0144 mmol) $[H\mathbf{1}H]^0$ in 2 mL of THF/MeCN (v/v = 1/1) was treated by *N,N*′-dimethylbenzimidazolium hexafluorophosphate[38] (5.0 mg, 0.0171 mmol). After 20 min, the solvent was removed under vacuum. The residue was dissolved in CD_2Cl_2 for NMR analysis. In the ^1H NMR spectrum, two singlets at δ 4.30 (2H, $-CH_3NCH_2NCH_3-$) and δ 2.72 (6H, $-CH_3NCH_2NCH_3-$) for 1,3-dimethylbenzimidazoline were observed; and a hydride signal was shown at −12.65 (m). ^{31}P NMR and IR spectra matched that for the two isomers of $[H\mathbf{1}(NCMe)]^+$.

Hydrogenation of Dimethyl Acetylenedicarboxylate with $[H\mathbf{1}H]^0$. A solution of $[H\mathbf{1}H]^0$ (10 mg, 0.01 mmol) in 5 mL of THF was frozen with liquid nitrogen. The atmosphere over the frozen solution was then filled with CO (6 psi). A sample of DMAD (~1.5 μL, 0.02 mmol) was injected. The mixture was allowed to warm to room temperature and stirred for a further 30 min. Solvent was removed under gentle vacuum, and hexane (5 mL × 3) was added to the green residue to extract organic compounds. The extracts were combined and dried under vacuum, and the oily residue was dissolved in $CDCl_3$ for ^1H NMR analysis. The ^1H NMR spectrum displays a

dx.doi.org/10.1021/ja501366j | J. Am. Chem. Soc. 2014, 136, 5773−5782

singlet at δ 6.27 for *cis*-$MeO_2CCH{=}CHCO_2Me$ (*note:* ^1H NMR for *trans*-$MeO_2CCH{=}CHCO_2Me$ is δ 6.86). IR and ^{31}P NMR analysis of the residue indicate that $[\mathbf{1}(CO)]$ was produced. When the same procedure was conducted using $[H\mathbf{1}H]^0$ and under an atmosphere of D_2, ^2H NMR analysis shows a singlet at δ 6.27 for *cis*-$MeO_2CCD{=}CDCO_2Me$.

DNMR Experiments. DNMR experiments were performed on a Varian Inova 600 MHz spectrometer equipped with a 5 mm AutoX dual broadband probe with *z*-gradient capability. The exchange rates of hydrides were measured by spin saturation transfer experiments.[39,40] A series of 50 spectra were collected with the saturation (selective irradiation) on either the bridging (δ −12.2) or the terminal hydride (δ −18.9) at different saturation times. The saturation times ranged from 0.002 to 2.5 s. The saturation power at 12 dB was chosen, which gave about 80% decrease of the signal with 1 s of saturation compared with a normal proton spectrum. The relaxation delay between pulses was 4.10 s. The intensity (integral) of the other hydride (the one not irradiated) was measured and was fitted to:

$$\frac{I(t)}{I(0)} = \frac{\tau^*}{\tau}\exp\left(\frac{-t}{\tau^*}\right) + \frac{\tau^*}{T_1}$$

where T_1 is the spin−lattice relaxation time of the hydride, τ is the lifetime of the exchanging hydride center, and $\tau^* = (T_1^{-1} + \tau^{-1})^{-1}$.

The spin−lattice relaxation times T_1 for the hydride signals at δ −12.2 and δ −18.9 were measured to be 0.748 and 0.644 s, respectively for $[H\mathbf{1}H]^0$ at −40 °C in THF-d_8 solution (sample concentration was 24 mM). For $[D\mathbf{1}D]^0$, the T_1 value for the signal at δ −12.2 was found to be 0.101 s.

The two-dimensional (2D) $^1H{-}^{31}P$ HMBC[41] spectra were collected at different multibond *J* values; the spectrum with *J* = 60 Hz is shown in Figure 4. In the 2D $^1H{-}^{31}P$ HMBC experiments, the spectral windows of ^1H and ^{31}P were set to 26991 and 14567 Hz, respectively. A total of 32 transients were acquired in the ^1H dimension and 100 transients were acquired in the ^{31}P dimension, using a relaxation delay of 1 s and acquisition time of 0.15 s. The spectra were processed with a 90°-shifted sine-bell square window function in Mnova 8.8.1 (Mestralab Research S.L.).

The 2D $^1H{-}^1H$ EXSY[39] (exchange spectroscopy) data were collected at different mixing times (0, and 100−1300 ms with 200 ms intervals). The spectrum with the mixing time of 500 ms is shown in the SI. In the 2D $^1H{-}^1H$ EXSY experiments, the spectral windows of ^1H in both dimensions were set to 26991 Hz. A total of 32 transients in the ^1H detection dimension and 200 transients in the second ^1H dimension with the relaxation delay of 1 s and acquisition time of 0.15 s were used. The spectra were processed with a 90°-shifted sine-bell square window function in Mnova 8.1.1.

Computational Details. Density functional theory (DFT) calculations were carried with the TURBOMOLE suite of programs.[42] High-quality level of theory (B-P86/TZVP[43]) was employed to treat explicitly (no effective core potential is used; inner shell electrons are explicitly treated). This DF scheme has been shown to be suitable for investigating hydrogenase models.[20,22,44]

All stationary points on the potential energy surface have been determined by means of energy gradient techniques, and a full vibrational analysis has been carried out to further characterize the nature of each point. Transition-state structures have been searched by means of a procedure based on a quasi-Newton−Josephson algorithm.[45] First, the geometry optimization of a guessed transition-state structure is carried out by freezing the molecular degrees of freedom corresponding to the reaction coordinate (RC). After performing the vibrational analysis of the constrained minimum energy structures, the negative eigenmode associated to the RC is followed to locate the true transition-state structure, which corresponds to the maximum energy point along the trajectory that joins two adjacent minima (i.e., reactants, products, and reaction intermediates).

In light of available experimental data and considering the nature of the ligands, only low-spin forms of FeFe complexes have been considered for DFT calculations. The Resolution of the Identity method[46] was used for approximating expensive four-center integrals (describing the classical electron−electron repulsive contribution to the total energy) through a combination of two three-center integrals. This procedure is made possible by expanding the density ρ in terms of an atom-centered and very large auxiliary basis set. IR simulations were performed with the same full-electron TZVP basis set that was employed to investigate energies and structures of isomeric forms of interest.

As for the DFT-calculated NMR data, the model was simplified by replacing Ph by methyl groups. The TZVP and TZVPP basis sets have been checked to provide approximately the same chemical shifts. Nuclear magnetic shielding tensors were computed using B-P86/TZVP geometries and the gauge including atomic orbital (GIAO) method.[47]

■ ASSOCIATED CONTENT

Supporting Information

^1H NMR and $^{31}P\{^1H\}$NMR spectra for new compounds. X-ray crystallographic data in CIF format. This material is available free of charge via the Internet at http://pubs.acs.org.

■ AUTHOR INFORMATION

Corresponding Authors

rauchfuz@illinois.edu (T.B.M.)

giuseppe.zampella@unimib.it (G.Z.)

Notes

The authors declare no competing financial interest.

■ ACKNOWLEDGMENTS

This research was conducted under contracts DEFG02-90ER14146 and DE-SC0001059 with the U.S. Department of Energy by its Division of Chemical Sciences, Office of Basic Energy Sciences.

■ REFERENCES

(1) Gloaguen, F.; Rauchfuss, T. B. *Chem. Soc. Rev.* **2009**, *38*, 100. Tard, C.; Pickett, C. J. *Chem. Rev.* **2009**, *109*, 2245.

(2) Vites, J.; Fehlner, T. P. *Organometallics* **1984**, *3*, 491.

(3) Carroll, M. E.; Barton, B. E.; Rauchfuss, T. B.; Carroll, P. J. *J. Am. Chem. Soc.* **2012**, *134*, 18843.

(4) van der Vlugt, J. I.; Rauchfuss, T. B.; Whaley, C. M.; Wilson, S. R. *J. Am. Chem. Soc.* **2005**, *127*, 16012.

(5) Nakazawa, H.; Itazaki, M. *Top. Organomet. Chem.* **2011**, *33*, 27.

(6) *Catalysis without Precious Metals*; Bullock, R. M., Ed.; Wiley-VCH: Weinheim, 2010; Bullock, R. M. *Science* **2013**, *342*, 1054.

(7) Ohki, Y.; Suzuki, H. *Angew. Chem., Int. Ed.* **2000**, *39*, 3120.

(8) Boncella, J. M.; Green, M. L. H.; O'Hare, D. *J, Chem. Soc., Chem. Commun.* **1986**, 618. Dapporto, P.; Midollini, S.; Sacconi, L. *Inorg. Chem.* **1975**, *14*, 1643.

(9) Smith, J. M.; Lachicotte, R. J.; Holland, P. L. *J. Am. Chem. Soc.* **2003**, *125*, 15752. Vela, J.; Smith, J. M.; Yu, Y.; Ketterer, N. A.; Flaschenriem, C. J.; Lachicotte, R. J.; Holland, P. L. *J. Am. Chem. Soc.* **2005**, *127*, 7857.

(10) Hoffman, B. M.; Lukoyanov, D.; Dean, D. R.; Seefeldt, L. C. *Acc. Chem. Res.* **2013**, *46*, 587.

(11) Dobbie, R. C.; Hopkinson, M. J.; Whittaker, D. *J. Chem. Soc., Dalton Trans.* **1972**, 1030. Cheah, M. H.; Borg, S. J.; Best, S. P. *Inorg. Chem.* **2007**, *46*, 1741.

(12) Tschierlei, S.; Ott, S.; Lomoth, R. *Energy Environ. Sci.* **2011**, *4*, 2340. Wang, M.; Chen, L.; Sun, L. *Energy Environ. Sci.* **2012**, *5*, 6763.

(13) Wang, W.; Nilges, M. J.; Rauchfuss, T. B.; Stein, M. *J. Am. Chem. Soc.* **2013**, *135*, 3633.

(14) Zhao, X.; Georgakaki, I. P.; Miller, M. L.; Mejia-Rodriguez, R.; Chiang, C.-Y.; Darensbourg, M. Y. *Inorg. Chem.* **2002**, *41*, 3917.

(15) de Leon, C. P.; Walsh, F. C.; Pletcher, D.; Browning, D. J.; Lakeman, J. B. *J. Power Sources* **2006**, *155*, 172.

(16) Justice, A. K.; Zampella, G.; De Gioia, L.; Rauchfuss, T. B.; van der Vlugt, J. I.; Wilson, S. R. *Inorg. Chem.* **2007**, *46*, 1655.
(17) Bampos, N.; Field, L. D.; Messerle, B. A. *Organometallics* **1993**, *12*, 2529.
(18) Gilbert-Wilson, R.; Field, L. D.; Colbran, S. B.; Bhadbhade, M. M. *Inorg. Chem.* **2013**, *52*, 3043.
(19) Zampella, G.; Bruschi, M.; Fantucci, P.; Razavet, M.; Pickett, C. J.; De Gioia, L. *Chem.—Eur. J.* **2005**, *11*, 509.
(20) Zampella, G.; Bruschi, M.; Fantucci, P.; De Gioia, L. *J. Am. Chem. Soc.* **2005**, *127*, 13180.
(21) Neugebauer, J.; Reiher, M.; Kind, C.; Hess, B. A. *J. Comput. Chem.* **2002**, *23*, 895.
(22) Zampella, G.; Fantucci, P.; De Gioia, L. *Chem. Commun.* **2010**, 8824.
(23) Martin, B. D.; Warner, K. E.; Norton, J. R. *J. Am. Chem. Soc.* **1986**, *108*, 33 This paper reminds us that the nucleophilicity and basicity of metal hydrides do not necessarily correlate.
(24) Cramer, C. J. *Essentials of Computational Chemistry*; John Wiley & Son: Hoboken, NJ, USA, 2002.
(25) Shapley, J. R.; Keister, J. B.; Churchill, M. R.; DeBoer, B. G. *J. Am. Chem. Soc.* **1975**, *97*, 4145.
(26) Perutz, R. N. *Pure Appl. Chem.* **1998**, *70*, 2211. Dugan, T. R.; Holland, P. L. *J. Organomet. Chem.* **2009**, *694*, 2825. Yu, Y.; Sadique, A. R.; Smith, J. M.; Dugan, T. R.; Cowley, R. E.; Brennessel, W. W.; Flaschenriem, C. J.; Bill, E.; Cundari, T. R.; Holland, P. L. *J. Am. Chem. Soc.* **2008**, *130*, 6624. Wong, K. S.; Fehlner, T. P. *J. Am. Chem. Soc.* **1981**, *103*, 966.
(27) Kütt, A.; Leito, I.; Kaljurand, I.; Soovali, L.; Vlasov, V. M.; Yagupolskii, L. M.; Koppel, I. A. *J. Org. Chem.* **2006**, *71*, 2829.
(28) Justice, A. K.; De Gioia, L.; Nilges, M. J.; Rauchfuss, T. B.; Wilson, S. R.; Zampella, G. *Inorg. Chem.* **2008**, *47*, 7405.
(29) Thomas, C. M.; Liu, T.; Hall, M. B.; Darensbourg, M. Y. *Inorg. Chem.* **2008**, *47*, 7009. Liu, T.; Darensbourg, M. Y. *J. Am. Chem. Soc.* **2007**, *129*, 7008. Justice, A. K.; Rauchfuss, T. B.; Wilson, S. R. *Angew. Chem., Int. Ed.* **2007**, *46*, 6152.
(30) Thomas, C. M.; Liu, T.; Hall, M. B.; Darensbourg, M. Y. *Chem. Commun.* **2008**, 1563.
(31) McSkimming, A.; Colbran, S. B. *Chem. Soc. Rev.* **2013**, *42*, 5439.
(32) Ezzaher, S.; Capon, J.-F.; Dumontet, N.; Gloaguen, F.; Pétillon, F. Y.; Schollhammer, P.; Talarmin, J. *J. Electroanal. Chem.* **2009**, *626*, 161.
(33) Bullock, R. M.; Bender, R. R. In *Encyclopedia of Catalysis*;Horvath, I. T., Ed.; Wiley-Interscience: Hoboken, NJ, 2003.
(34) Shima, S.; Ermler, U. *Eur. J. Inorg. Chem.* **2011**, *2011*, 963.
(35) Camara, J. M.; Rauchfuss, T. B. *Nat. Chem.* **2012**, *4*, 26.
(36) Smith, K.-T.; Tilset, M.; Kuhlman, R.; Caulton, K. G. *J. Am. Chem. Soc.* **1995**, *117*, 9473.
(37) Parkin, A.; Cavazza, C.; Fontecilla-Camps, J. C.; Armstrong, F. A. *J. Am. Chem. Soc.* **2006**, *128*, 16808. Chen, Z.; Lemon, B. J.; Huang, S.; Swartz, D. J.; Peters, J. W.; Bagley, K. A. *Biochemistry* **2002**, *41*, 2036.
(38) Zhu, X.-Q.; Zhang, M.-T.; Yu, A.; Wang, C.-H.; Cheng, J.-P. *J. Am. Chem. Soc.* **2008**, *130*, 2501.
(39) Friebolin, H. *Basic One- and Two-Dimensional NMR Spectroscopy*, 4th ed.; VCH: Weinheim, 2008.
(40) Jarek, R. L.; Flesher, R. J.; Shin, S. K. *J. Chem. Educ.* **1997**, *74*, 978.
(41) Bax, A.; Summers, M. F. *J. Am. Chem. Soc.* **1986**, *108*, 2093.
(42) Ahlrichs, R.; Baer, M.; Haeser, M.; Horn, H.; Koelmel, C. *Chem. Phys. Lett.* **1989**, *162*, 165.
(43) Becke, A. D. *Phys. Rev. A* **1988**, *38*, 3098. Perdew, J. P. *Phys. Rev. B* **1986**, *33*, 8822.
(44) Bertini, L.; Greco, C.; Bruschi, M.; Fantucci, P.; De Gioia, L. *Organometallics* **2010**, *29*, 2013. Siegbahn, P. E. M.; Tye, J. W.; Hall, M. B. *Chem. Rev.* **2007**, *107*, 4414. Zampella, G.; Greco, C.; Fantucci, P.; De Gioia, L. *Inorg. Chem.* **2006**, *45*, 4109. Zampella, G.; Fantucci, P.; De Gioia, L. *J. Am. Chem. Soc.* **2009**, *131*, 10909.
(45) Jensen, F. *Introduction to Computational Chemistry*; Wiley: Chichester, UK, 2007.
(46) Eichkorn, K.; Weigend, F.; Treutler, O.; Ahlrichs, R. *Theor. Chem. Acc.* **1997**, *97*, 119.
(47) Ditchfield, R. *Mol. Phys.* **1974**, *27*, 789. Wolinski, K.; Hinton, J. F.; Pulay, P. *J. Am. Chem. Soc.* **1990**, *112*, 8251.